# Iterative Non-Stationary Channel Estimation for LTE Downlink Communications

Markus Hofer, Thomas Zemen
FTW Forschungszentrum Telekommunikation Wien, Vienna, Austria
Email: {markus.hofer, thomas.zemen}@ftw.at

***Abstract*—Intelligent transport systems (ITS) require low-latency dependable wireless communication links between transmitter and receiver. In vehicular communication scenarios communication channels are highly dispersive which makes the design of appropriate channel estimators especially difficult. In this paper we address the problem of non-stationary vehicular channel estimation for 3GPP long term evolution (LTE) which is recently investigated for its usability in ITS applications. We present an iterative reduced-rank channel estimator for the LTE downlink utilizing a subspace representation based on discrete prolate spheroidal sequences. The subspace is adapted to the time-varying delay and Doppler-spread for each received frame with a hypothesis test. This hypothesis test is adapted to the specific pilot grid in LTE. With this setup we can achieve a twofold reduction in the number of required iterations to achieve a frame error rate (FER) below $10^{-1}$ for a relative velocity range of 0 to 400 km/h, a delay spread of 0 to 4.7 $\mu$s at a signal-to-noise ratio (SNR) of 13 dB.**

***Index Terms*—long term evolution, discrete prolate spheroidal sequences, iterative channel estimation, D2D communication**

## I. Introduction

Low-latency dependable wireless vehicular communication is an important building block for intelligent transport system (ITS) [1] to reduce the number of casualties on the road. Besides 802.11p [2] also 3GPP long term evolution (LTE) [3] is recently investigated as potential candidate for ITS applications [4]. LTE offers a large coverage area, high capacity and high penentration to face the well known drawbacks of 802.11p of poor scalability, low capacity and intermittent connectivity [4].

For reliable vehicular communication, channel estimation methods are required that can deal with high delay- and Doppler spreads in non-stationary propagation conditions, i.e. the delay and Doppler spread changes over time [5–7].

A robust reduced-rank iterative channel estimator that relies on a correlation matrix assuming a flat delay-Doppler scattering function was presented in [8, 9]. The support region of the scattering function is defined by the maximum delay-spread and the maximum Doppler-spread of the channel. The eigenvectors of the channels autocorrelation matrix can be approximated by a two dimensional subspace model using generalized discrete prolate spheroidal (DPS) sequences [10, 11]. Such an approach is mismatched to the actual support of the scattering function.

To improve the performance, an adaptive subspace selection algorithm that estimates the actual delay and Doppler support of the current channel realization is presented in [12] for the specific pilot pattern of the IEEE 802.11p [2] standard. This pilot pattern provides a contiguous pilot grid in time and frequency which is a crucial requirement for the subspace selection algorithm [13]. The LTE downlink pilot pattern is non contiguous which means the subspace selection algorithm presented in [13] cannot be directly utilized.

*Contributions of the Paper:* (a) We present an adaptive subspace selection algorithm [12] for a non-contiguous, equidistant pilot grid and provide a performance evaluation based on numerical simulation results for doubly-selective channels. (b) We extend the iterative reduced-rank channel estimation algorithm of [9, 12] to higher order modulation alphabets.

Since the presented channel estimator adapts to the channel statistic on a *per frame basis* this estimation technique would also be applicable to LTE device-to-device (D2D) communication if the LTE downlink pilot pattern is utilized. This could significantly reduce the latency of vehicular-to-vehicular communication links which otherwise would have to communicate via the basestation.

## II. System Model

For the system model we assume a modulation scheme based on a single-input single-output (SISO) LTE downlink (see Fig 1).

An information bit stream $\epsilon[m'']$ is turbo encoded, interleaved and rate matched resulting in the coded bit stream $c[m']$. Subsequently, $c[m']$ is partitioned into vectors $\mathbf{t} = (t_1, t_2, \ldots, t_Q)$ of length $Q$, which are converted to complex data symbols $b$ utilizing either a 4-, 16- or 64-QAM symbol alphabet [14, Sec. 7.1]. The data symbols are mapped to the orthogonal frequency division multiplexing (OFDM) time-frequency grid of an LTE subframe. Each subframe has a duration of 1 ms in the time domain and, depending on the overall system bandwidth, consists of 6 up to 100 resource block pairs (RBPs) $N_{\text{RBP}}$ in the frequency domain. The RBP is the minimum scheduling unit in LTE. For a normal cyclic prefix (CP) length a RBP entails 14 OFDM symbols in the time direction and 12 subcarries in the frequency direction. The time-frequency grid for a subframe with normal CP length is shown in Fig. 2.

Pilot symbols $p[m, q]$ are inserted in the time-frequency grid to estimate the channels time-frequency response, where $m \in \{0, \ldots, M-1\}$ denotes the discrete time and $q \in \{0, \ldots, N-1\}$ the discrete frequency. The size of the $M$ and $N$ depend on the number of considered subframes and the number of

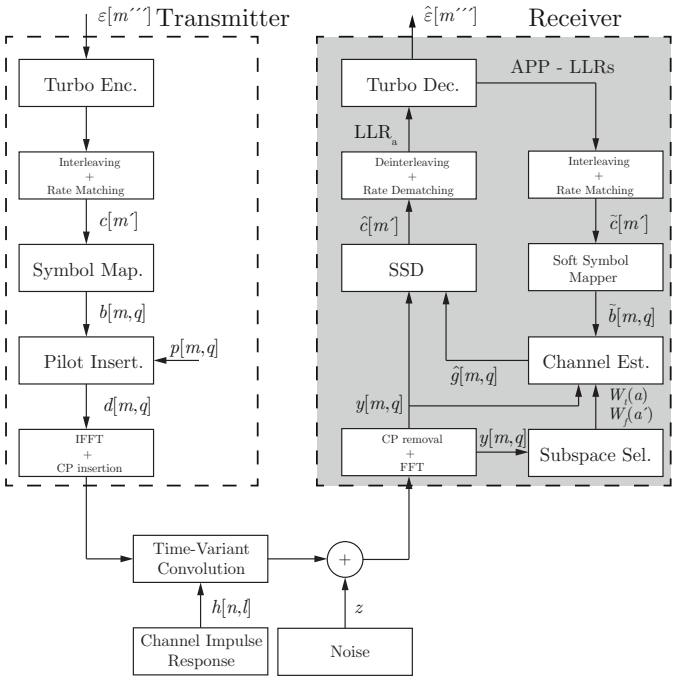


Fig. 1. SISO LTE downlink system model

RBPs within one subframe. The pilot symbols are element of a 4-QAM symbol alphabet and assumed to be known to the receiver.

The multiplexing operation of data and pilot symbols can be described as

$$d[m,q] = b[m,q] + p[m,q]. \tag{1}$$

where $b[m,q]$ denotes the coded data symbols. The data symbol positions are defined by the two dimensional index set $\mathcal{S}$, while the pilot symbol positions are defined by the two dimensional index set $\mathcal{P}$. The two index sets are complementary, i.e., $\mathcal{S} \cap \mathcal{P} = 0$, or $b[m,q] = 0 \,\forall\, (m,q) \notin \mathcal{S}$ and vice versa. After inverse fast Fourier transform (IFFT) and CP insertion the signal is transmitted over a time-variant frequency-selective channel $h(t,\tau)$, where $t$ represents the time and $\tau$ the delay. The discretized channel impulse response can be represented by

$$h[n,l] := h(nT_c, lT_c). \tag{2}$$

Here, $n$ denotes the discrete time index, $l$ the discrete frequency index, both at rate $R_C = 1/T_C$ and $T_C$ the chip duration. The chiprate $R_C$ is defined by $R_C = N' \cdot f_\Delta$, where $N'$ is the FFT size and $f_\Delta = 15\,\text{kHz}$ the subcarrier spacing. We assume that the time-variant channel impulse response has a maximum support of $0 \le l \le L-1$ with $L = \lceil \tau_{\text{Pmax}}/T_C \rceil$ where $\tau_{\text{Pmax}}$ denotes the maximum path delay. To avoid inter-symbol interference (ISI) the maximum path delay is restricted to be shorter than or equal to the CP length of the OFDM symbols. We assume that for the considered scenario the inter-carrier interference (ICI) has only a minor impact on the receiver performance. In this case, after fast Fourier transform (FFT) and CP removal, the received signal $y[m,q]$ can be modeled as

$$y[m,q] = g[m,q]d[m,q] + z[m,q], \tag{3}$$

where the channel coefficient $g[m,q]$ is the FFT of $h[n,l]$ sampled at $h[m(N'+L)+L+N'/2,l]$ and $z[m,q] \sim \mathcal{CN}(0,\sigma_z^2)$ the symmetric complex additive white Gaussian noise with zero mean and covariance $\sigma_z^2$, respectively.

The received signal is input to a max-log soft sphere decoder (SSD) [15] that uses the estimated channel coefficients $\hat{g}[m,q]$ to generate the log-likelihood ratios (LLRs) of the encoded data bits $\hat{c}[m']$. After rate-dematching and deinterleaving the LLRs are fed to the turbo decoder. The turbo decoder generates the (a posteriori) LLRs of the information bit stream, which, after hard decision, results in a received information bit stream $\hat{\epsilon}[m'']$ and the (a posteriori) LLRs of the encoded data bits which are utilized as soft information feedback to improve the channel estimator performance.

## III. Iterative Channel Estimation

To obtain the estimated channel coefficients $\hat{g}[m,q]$ we use an iterative channel estimator. The LLRs obtained by the turbo decoder are utilized as a priori information to generate soft symbol feedback that is used to improve the estimator performance in each iteration step. Defining the $NM \times 1$ sized received vector $\mathbf{y}$ by

$$\mathbf{y} = [y[0,0], y[0,1], \ldots, y[0,N-1], \ldots, y[M-1,0], y[M-1,1], \ldots, y[M-1,N-1]]^T \tag{4}$$

we can rewrite (3) in matrix-vector form according to

$$\mathbf{y} = \mathbf{D}\mathbf{g} + \mathbf{z}. \tag{5}$$

The channel vector $\mathbf{g}$, symbol vector $\mathbf{d}$ and noise vector $\mathbf{z}$ are defined similarly to (4) and $\mathbf{D} = \text{diag}(\mathbf{d})$ is a size $NM \times NM$ diagonal matrix. To incorporate the soft symbol feedback we substitute $\mathbf{D}$ in (5) by $\tilde{\mathbf{D}} = \text{diag}(\tilde{\mathbf{d}})$. The $NM \times 1$ sized vector $\tilde{\mathbf{d}}$ has the elements

$$\tilde{d}[m,q] = \tilde{b}[m,q] + p[m,q], \tag{6}$$

and $\tilde{b}[m,q]$ are the soft data symbols on the index set $\mathcal{S}$ that are obtained from the rate-matched, interleaved LLRs of the turbo decoder.

### A. Wiener Filter

To estimate the channel vector $\mathbf{g}$ we use a linear minimum mean square error (LMMSE) estimator. Following the derivation in [16, (36)-(39)] we obtain the well known Wiener-Filter

$$\hat{\mathbf{g}} = \mathbf{R}_\mathbf{g}\tilde{\mathbf{D}}^H \left(\tilde{\mathbf{D}}\mathbf{R}_\mathbf{g}\tilde{\mathbf{D}}^H + \mathbf{\Lambda} + \sigma_z^2\mathbf{I}_{NM}\right)^{-1}\mathbf{y}, \tag{7}$$

that provides the channel estimate $\hat{\mathbf{g}}$. Here, $(\cdot)^H$ is the conjugate transpose, $\mathbf{R}_g = E\{\mathbf{g}\mathbf{g}^H\}$ is the channel autocorrelation matrix (c.f. Section III-B), $\mathbf{I}_{NM}$ is the identity matrix, and $\mathbf{\Lambda}$ is a diagonal matrix that incorporates the variances of the symbols $\tilde{d}[m,q]$. All matrices are of size $NM \times NM$. The elements $\mathbf{\Lambda}$ are calculated by

$$[\mathbf{\Lambda}]_{m+Mq,m+Mq} = [\mathbf{R}_\mathbf{g}]_{m+Mq,m+Mq}\sigma^2_{\tilde{d}[m,q]} \tag{8}$$

with $\sigma^2_{\tilde{d}[m,q]}$ denoting the variance of $\tilde{d}[m,q]$. The entries on the diagonal of $\mathbf{\Lambda}$ are zero for pilot positions $(m,q) \in \mathcal{P}$

since $\sigma_{p[m,q]} = 0$ for the known pilot symbols. In the first iteration loop no LLR information is available and only the pilot symbols are used for channel estimation, i.e., $\tilde{d}[m,q] = 0$ and $\sigma^2_{\tilde{d}[m,q]} = 1 \,\forall\, (m,q) \in \mathcal{S}$. From the second iteration on, we utilize the pilot symbols $p[m,q]$ and the soft data symbols $\tilde{b}[m,q]$ for channel estimation.

To calculate the soft data symbols $\tilde{b}[m,q]$ and variances $\sigma^2_{\tilde{b}[m,q]}$ on the data symbol positions $(m,q) \in \mathcal{S}$ we partition the LLR stream $\tilde{c}[m']$ into vectors $\mathbf{c} = (c_1, c_2, \ldots, c_Q)$ of size $Q$ which contain the LLRs of the corresponding bit vector $\mathbf{t} = (t_1, t_2, \ldots, t_Q)$. Neglecting for the sake of simplicity the mapping indices $(m,q)$, the soft data symbols and variances are calculated according to [17]

$$\tilde{b} = \overline{b} = \sum_{b_i \in \mathcal{B}} b_i \cdot P(b = b_i), \tag{9}$$

$$\sigma^2_{\tilde{b}} = \left( \sum_{b_i \in \mathcal{B}} |b_i|^2 \cdot P(b = b_i) \right) - |\tilde{b}|^2, \tag{10}$$

where $b_i$ is the $i$-th symbol within the utilized symbol alphabet $\mathcal{B}$ (4-,16- or 64-QAM) and each $b_i \in \mathcal{B}$ corresponds to $Q$ bits $\mathbf{t}_i = (t_{i,1}, \ldots, t_{i,Q})$.

If we assume that due to interleaving the data bits $\mathbf{t}$ are independent, the symbol probabilities $P(b = b_i)$ are calculated according to [17]

$$P(b = b_i) = \prod_{j=1}^{Q} \frac{1 + \tilde{t}_{i,j} u_j}{2} \tag{11}$$

Here $t_{i,j}$ is the $j$-th data bit of the symbol $b_i$ and

$$\tilde{t}_{i,j} = \begin{cases} +1, & t_{i,j} = 0 \\ -1, & t_{i,j} = 1 \end{cases} \tag{12}$$

The variable $u_j = \tanh(c_j/2)$ is obtained by the hyperbolic tangent of the LLR of the corresponding data bit $t_j$.

Taking the bit-symbol mapping of [3, Sec 7.1.2 - 7.1.4] into account we can simplify the calculation of the symbol statistics and obtain

*1) 4-QAM:*

$$\tilde{b} = \frac{u_1 + j \cdot u_2}{\sqrt{2}} \tag{13}$$

$$\sigma^2_{\tilde{b}} = 1 - |\tilde{d}|^2 \tag{14}$$

*2) 16-QAM:*

$$\tilde{b} = \frac{(2u_1 - u_1 u_3) + j \cdot (2u_2 - u_2 u4)}{\sqrt{10}} \tag{15}$$

$$\sigma^2_{\tilde{b}} = 1 - \frac{2}{5}(u_3 + u_4) - |\tilde{d}|^2 \tag{16}$$

*3) 64-QAM:*

$$\tilde{b} = \frac{u_1(4 - u_3(2 - u_5)) + j \cdot u_2(4 - u_4(2 - u_6))}{\sqrt{42}} \tag{17}$$

$$\sigma^2_{\tilde{b}} = 1 + \frac{2}{21}(u_6(2u_4 - 1) + u_5(2u_3 - 1)) - \frac{8}{21}(u_3 + u_4) - |\tilde{d}|^2 \tag{18}$$

These calculations were also performed in [18], however there is an sign error in the calculation of the variances of the 64-QAM alphabet.

### *B. Robust Reduced Rank Approximation*

The channel autocorrelation matrix $\mathbf{R_g}$ is in general not known to the receiver. To circumvent this problem we approximate the autocorrelation matrix $\mathbf{R_g}$ in (7) by a robust autocorrelation matrix $\tilde{\mathbf{R}}_\mathbf{g}$ that assumes a flat delay-Doppler scattering function within a two dimensional support region

$$\mathcal{W} = W_f \times W_t = [-\nu_\mathrm{D}, \nu_\mathrm{D}] \times [0, \theta_\mathrm{P}]. \tag{19}$$

In detail $W_t$ defines the support region of the Doppler power spectral density (DSD) with $0 \leq \nu_\mathrm{D} \leq \nu_\mathrm{Dmax}$ and $W_f$ defines the support region of the power-delay profile (PDP) with $0 \leq \theta_\mathrm{P} \leq \theta_\mathrm{Pmax}$. The only required parameters to calculate $\mathbf{R_g}$ are the normalized Doppler bandwidth $\nu_\mathrm{D} = f_\mathrm{D} T_S$ and the normalized delay $\theta_\mathrm{P} = \tau_\mathrm{P}/(N' T_C)$ which are obtained by the hypothesis test presented in Section IV. The variable $f_\mathrm{D}$ denotes the Doppler frequency, $T_S$ the OFDM symbol duration, $\tau_\mathrm{P}$ the path delay, $N'$ the FFT size and $T_C$ the chip-duration of the system. The Doppler frequency is obtained by $f_\mathrm{D} = v/c_0 \cdot f_C$, with $v$ the relative velocity between transmitter and receiver, $c_0$ the speed of light and $f_C$ the carrier frequency of the system. For a finite sized hypothesis test all relevant matrices can be precalculated and stored which significantly reduces the complexity.

For a autocorrelation matrix with flat delay-Doppler support the eigenvectors $\mathbf{U}(\mathcal{W}, \mathcal{I})$ of

$$\tilde{\mathbf{R}}_\mathbf{g} = \mathbf{U}(\mathcal{W}, \mathcal{I}) \mathbf{\Sigma}(\mathcal{W}, \mathcal{I}) \mathbf{U}(\mathcal{W}, \mathcal{I})^H, \tag{20}$$

are also spanned by the two dimensional subspace of DPS sequences where $\mathbf{\Sigma}(\mathcal{W}, \mathcal{I})$ is the diagonal matrix of eigenvalues and $\mathcal{I} = I_t \times I_f = [0, \ldots, M-1] \times [-N/2, \ldots, N/2 - 1]$ is the finite index set where the fading process is observed on. Specifically, we can factorize

$$\tilde{\mathbf{R}}_\mathbf{g} = \mathbf{R}(W_t, I_t) \otimes \mathbf{R}(W_f, I_f), \tag{21}$$

with $\otimes$ denoting the Kronecker product. The eigenvectors $\mathbf{U}(W, I)$ of the autocorrelation matrix $\mathbf{R}(W, I)$ are generalized DPS sequences [12] allowing to calculate $\mathbf{U}(\mathcal{W}, \mathcal{I})$ by

$$\mathbf{U} = \mathbf{U}(\mathcal{W}, \mathcal{I}) = \Pi(\mathbf{U}(W_t, I_t) \diamond \mathbf{U}(W_f, I_f)), \tag{22}$$

where the operator $\diamond$ is the Tracy-Singh product of column-wise partitioned matrices [12]. The diagonal matrix $\mathbf{\Sigma}$ is obtained by

$$\mathbf{\Sigma} = \mathbf{\Sigma}(\mathcal{W}, \mathcal{I}) = \Pi(\mathrm{diag}(\boldsymbol{\sigma}(W_t, I_t) \otimes \boldsymbol{\sigma}(W_f, I_f))), \tag{23}$$

and $\boldsymbol{\sigma}(W, I)$ are the eigenvalues of $\mathbf{R}(W, I)$. The permutation operator $\Pi(\cdot)$ ensures that the columns of $\mathbf{\Sigma}$ (and $\mathbf{U}$) are sorted from biggest to smallest eigenvalue, i.e., $\lambda_0(\mathcal{W}, \mathcal{I}) \geq \lambda_1(\mathcal{W}, \mathcal{I}) \geq \ldots \geq \lambda_{|\mathcal{I}|-1}(\mathcal{W}, \mathcal{I})$. The eigenvalue matrix $\mathbf{\Sigma}$ has only $D$ dominant eigenvalues which allows us to approximate $\tilde{\mathbf{R}}_\mathbf{g}$ by a robust reduced-rank matrix $\tilde{\mathbf{R}}_\mathbf{g} \approx \breve{\mathbf{R}}_\mathbf{g} = \mathbf{U}_D \mathbf{\Sigma}_D \mathbf{U}_D^H$ where $\mathbf{U}_D$ and $\mathbf{\Sigma}_D$ contain the first $D$ columns of $\mathbf{U}$ and $\mathbf{\Sigma}$, respectively. The dimension $D$ is obtained by

$$D = \underset{\mathcal{D} \in \{1, \ldots, |\mathcal{I}|\}}{\operatorname{argmin}} \left( \frac{1}{|\mathcal{W}||\mathcal{I}|} \sum_{i=\mathcal{D}}^{|\mathcal{I}|-1} \lambda_i(\mathcal{W}, \mathcal{I}) + \frac{\mathcal{D}}{|\mathcal{I}|} \sigma_z^2 \right). \tag{24}$$

Inserting $\breve{\mathbf{R}}_\mathbf{g}$ in (7) allows for further significant complexity reduction.

## IV. Adaptive Subspace Selection for a Non-Contiguous Equidistant Pilot Grid

Approximating the autocorrelation matrix $\mathbf{R_g}$ with a robust autocorrelation matrix $\tilde{\mathbf{R}}_\mathbf{g}$ that assumes maximum Doppler support $\nu_{\text{Dmax}}$ and delay support $\theta_{\text{Pmax}}$ would obviously lead to a mismatch to the current channel realization. To improve the performance we use a frame based hypothesis test [11, 12] that utilizes the observations at the pilot positions $\mathcal{P}$ to estimate the support of the DSD $W_t = [-\nu_\text{D}, \nu_\text{D}] \subset [-\nu_{\text{Dmax}}, \nu_{\text{Dmax}}]$ and the support of the PDP $W_f = [0, \theta_\text{P}] \subset [0, \theta_{\text{Pmax}}]$. We define a finite set of $A = 10$ hypotheses $\{W_t(1), \dots, W_t(a), \dots, W_t(A)\}$ on the DSD support with $W_t(a) = (-a/A \cdot \nu_{\text{Dmax}}, a/A \cdot \nu_{\text{Dmax}})$ and a finite set of $A' = 10$ hypotheses $\{W_f(1), \dots, W_f(a'), \dots, W_f(A')\}$ on the PDP support with $W_f(a') = (0, a'/A' \cdot \theta_{\text{Pmax}})$. The hypothesis test provides a hypothesis set combination $(a, a')$ that fits the normalized Doppler bandwidth $\nu_\text{D}$ and delay $\theta_\text{P}$ of the current channel realization best. Each hypothesis represents a subspace spanned by the columns of $\mathbf{U}(W_t(a), I_t)$ for $a \in \{1, \dots A\}$ and $\mathbf{U}(W_f(a'), I_f)$ for $a' \in \{1, \dots A'\}$ and their corresponding eigenvalue matrices. These matrices can be precalculated and stored. Utilizing Equations (20)–(23) we can calculate $\tilde{\mathbf{R}}_\mathbf{g}$ for the Wiener filter in (7). Performing rank-reduction using (24) we can save substantial complexity.

For the hypothesis test we define the signal model for channel estimation only at the pilot positions $\mathcal{P}$

$$\mathbf{y}^{(\mathcal{P})} = \mathbf{D}^{(\mathcal{P})}\mathbf{g}^{(\mathcal{P})} + \mathbf{z}^{(\mathcal{P})}, \tag{25}$$

with $\mathbf{D}^{(\mathcal{P})} = \text{diag}(\mathbf{d}^{(\mathcal{P})})$, where $\mathbf{y}^{(\mathcal{P})}, \mathbf{d}^{(\mathcal{P})}, \mathbf{g}^{(\mathcal{P})}$ and $\mathbf{z}^{(\mathcal{P})}$ contain the respective elements for $(m, q) \in \mathcal{P}$ sorted in the same order as $\mathbf{y}$ in (4). The correlated 2-D observations at the pilot positions $\mathcal{P}$ are obtained according to

$$\mathbf{w}^{(\mathcal{P})} = {\mathbf{D}^{(\mathcal{P})}}^H \mathbf{y}^{(\mathcal{P})} = \mathbf{g}^{(\mathcal{P})} + {\mathbf{D}^{(\mathcal{P})}}^H \mathbf{z}^{(\mathcal{P})} = \mathbf{g}^{(\mathcal{P})} + \mathbf{z}'^{(\mathcal{P})} \tag{26}$$

where $\mathbf{z}'^{(\mathcal{P})} \sim \mathcal{CN}(0, \sigma_z^2 \mathbf{I}_{|\mathcal{P}|})$ has the same statistics as $\mathbf{z}^{(\mathcal{P})}$. The fading process observed on the pilot symbols $\mathcal{P}$ can also be described by the eigenvectors $\mathbf{U}^{(\mathcal{P})}$ of the autocorrelation matrix

$$\tilde{\mathbf{R}}_{\mathbf{g}^{(\mathcal{P})}} = E\left\{\mathbf{g}^{(\mathcal{P})} {\mathbf{g}^{(\mathcal{P})}}^H\right\}. \tag{27}$$

For $\tilde{\mathbf{R}}_{\mathbf{g}^{(\mathcal{P})}}$ we assume a flat delay-Doppler scattering function. We use the eigenvectors $\mathbf{U}^{(\mathcal{P})}$ to perform the hypothesis test which selects the support that fits best for the current channel realization.

Since the condition number of $\tilde{\mathbf{R}}_{\mathbf{g}^{(\mathcal{P})}}$ is high and $\mathcal{P}$ cannot directly be factorized in a Cartesian product we cannot use the eigenvectors obtained by regular decomposition methods to setup the subspaces for the hypothesis test. Furthermore, we cannot use DPS sequences directly for the subspace setup of $\mathbf{U}^{(\mathcal{P})}$ since they are solely defined on a contiguous pilot pattern. Our novel solution to this problem is as follows: We partition $\mathcal{P}$ into two two-dimensional index sets $\mathcal{I}_a$ and $\mathcal{I}_b$ both of size $2 \cdot N_{\text{SUBF}} \times 2 \cdot N_{\text{RBP}}$ (see Fig. 2). Each of these index sets is defined as a Cartesian product of an index set in the time and the frequency domain according to

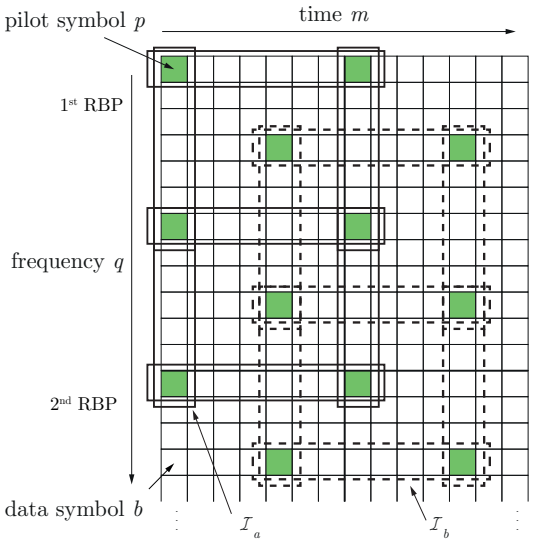


Fig. 2. OFDM time-frequency grid of one LTE subframe with normal CP length and partitioned index sets $\mathcal{I}_a$ and $\mathcal{I}_b$

$$\mathcal{I}_a = I_{a_t} \times I_{a_f} \quad \text{and} \quad \mathcal{I}_b = I_{b_t} \times I_{b_f} \tag{28}$$

The time index sets are defined by

$$I_{a_t} = \Delta_t \cdot k_t + 1 \quad \text{and} \quad I_{b_t} = I_{a_t} + \Delta x, \tag{29}$$

with $k_t \in \{0, 1, \dots, 2 \cdot N_{\text{SUBF}} - 1\}$, $\Delta_t = 7$ the distance between the pilot symbols in time, $\Delta x = 4$ the shift of $I_{b_t}$ against $I_{a_t}$ and $N_{\text{SUBF}}$ is the number of considered subframes. The frequency index sets are defined by

$$I_{a_f} = \Delta_f \cdot k_f + 1 \quad \text{and} \quad I_{b_f} = I_{a_f} + \Delta y \tag{30}$$

with $k_f \in \{0, 1, \dots, 2 \cdot N_{\text{RBP}} - 1\}$, $\Delta_f = 6$ the distance between the pilot symbols in frequency, $\Delta y = 2$ the shift of $I_{b_f}$ against $I_{a_f}$ and $N_{\text{RBP}}$ the number of RBPs that depend on the bandwidth.

The two pilot index sets contain equidistant elements, where the distance in time is $\Delta_t$ and $\Delta_f$ in frequency. We assume that the fading process is wide-sense stationary within the considered observation region [7]. Because of the equidistant pilot structure of the index grids the eigenvector matrices $\mathbf{U}(W_t(a), I_{a_t})$ and $\mathbf{U}(W_f(a'), I_{a_f})$ can now be obtained from generalized DPS sequences. We set $\nu'_\text{D} = \Delta_t \nu_\text{D}$ and $\theta'_\text{P} = \Delta_f \theta_\text{P}$ and use [12, Eq. (20)-(25)] to obtain the eigenvector matrices. Then we use (22) to obtain $\mathbf{U}^{(\mathcal{I}_a)}$. Obviously, the autocorrelation matrix of $\mathcal{I}_b$ and $\mathcal{I}_a$ are equal since $\mathcal{I}_b$ is only a shift of $\mathcal{I}_a$ by $(\Delta x, \Delta y)$, i.e., $\mathbf{U}^{(\mathcal{I}_b)} = \mathbf{U}^{(\mathcal{I}_a)}$. For the selection of the correct subspace we use $\mathbf{U}^{(\mathcal{I}_a)}$ and $\mathbf{U}^{(\mathcal{I}_b)}$ separately to calculate the channel estimates on the index sets according to (e.g. shown for $\mathcal{I}_a$)

$$\hat{\mathbf{g}}^{(\mathcal{I}_a)} = \mathbf{U}^{(\mathcal{I}_a)} {\mathbf{U}^{(\mathcal{I}_a)}}^H \mathbf{w}^{(\mathcal{I}_a)} \tag{31}$$

The channel estimates are utilized to obtain the data errors $x^{(\mathcal{I}_a)}$ and $x^{(\mathcal{I}_b)}$ by (e.g. for the data error on $\mathcal{I}_a$)

$$x^{(\mathcal{I}_a)} = \frac{1}{|\mathcal{I}_a|} ||\mathbf{w}^{(\mathcal{I}_a)} - \hat{\mathbf{g}}^{(\mathcal{I}_a)}||^2 \tag{32}$$

which are averaged and then the hypothesis test is performed according to [12, Eq. (43)-(48)].

## V. Simulation Results

In this section we evaluate the performance of the adaptive subspace selection algorithm. For the numerical simulations we employ a Rayleigh fading channel model with exponentially decaying PDP within the normalized support $[0, \theta_{\mathrm{P}}]$ and normalized root mean square (RMS) delay spread $\theta_{\mathrm{P}}/5$. Time selective fading is calculated per tap according to a Clarke's model giving a normalized Doppler bandwidth $\nu_{\mathrm{D}}$. For the system bandwidth we choose $B = 1.4\,\mathrm{MHz}$ which is equal to $N_{\mathrm{RBP}} = 6$ or $N = 12 \cdot N_{\mathrm{RBP}} = 72$ data subcarriers. We simulate frames with $N_{\mathrm{SUBF}} = 1$ or 2 subframes and $M = 14 \cdot N_{\mathrm{SUBF}}$. For the simulations we assume that the user occupies the whole available transmission bandwidth $B$. We set the carrier frequency to $f_C = 2.6\,\mathrm{GHz}$ and the FFT size to $N' = 128$. The OFDM symbol duration including CP is $T_S \approx 71.4\,\mu\mathrm{s}$. The maximum relative velocity between transmitter and receiver is $v_{\max} = 400\,\mathrm{km/h} = 111.11\mathrm{m/s}$ and the maximum path delay is assumed with $\tau_{\mathrm{Pmax}} = 4.7\,\mu\mathrm{s}$ which is the smallest CP duration for normal CP length. This results in a maximum normalized one sided Doppler bandwidth of $\nu_{\mathrm{Dmax}} = 0.0688$ and maximum normalized path delay $\theta_{\mathrm{Pmax}} = 0.0703$.

To evaluate the performance of the time domain subspace selection algorithm we generate a time-frequency selective fading process. We set the PDP support to $\theta_{\mathrm{P}} = \theta_{\mathrm{Pmax}}$ and vary the Doppler bandwidth $\nu_{\mathrm{D}}$ within $0 \leq \nu_{\mathrm{D}} \leq \nu_{\mathrm{Dmax}}$. This relates to a velocity range $v \in (0, 111.1)\,\mathrm{m/s} \approx (0, 400)\,\mathrm{km/h}$. For the simulations we simulate 500 frames for each $\nu_{\mathrm{D}}$ value. Figure 3 depicts the channel estimation mean square error (MSE) on the pilot index set $\mathcal{P}$ for different Doppler bandwidths $\nu_{\mathrm{D}}$ and fixed SNR $\in \{0, 10\}$ dB. We show the MSE obtained by the adaptive subspace selection algorithm. Furthermore, we present the MSE if we select the largest subspace and the MSE if we assume $v_{\mathrm{D}}$ and the corresponding subspace as perfectly known. The solid lines refer to the results obtained if the user is scheduled for only one subframe in time. The gain in MSE

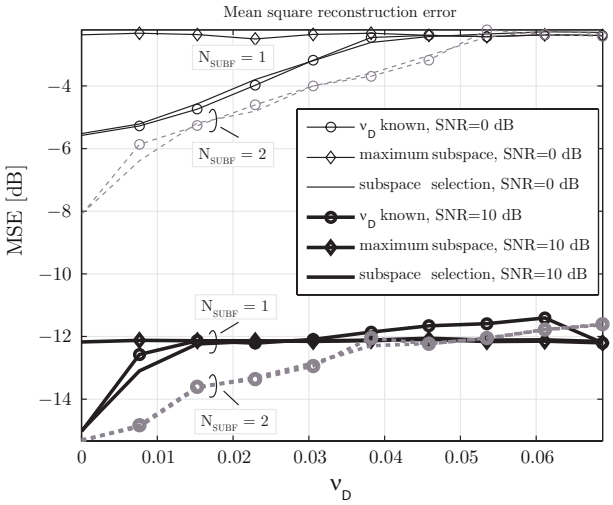


Fig. 3. MSE vs. Doppler bandwidth $\nu_{\mathrm{D}}$ for SNR $\in \{0, 10\}$ dB for adaptive subspace selection in the time domain with $N_{\mathrm{SUBF}} \in \{1, 2\}$

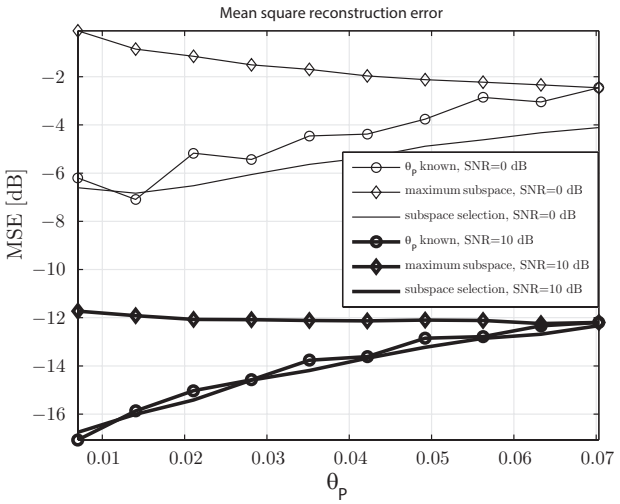


Fig. 4. MSE vs. normalized PDP support $\theta_{\mathrm{P}}$ for SNR $\in \{0, 10\}$ dB for adaptive subspace selection in the frequency domain

of the subspace selection compared to the maximum subspace is around 3 dB for low velocities and the performance of the subspace selection follows closely the performance for known $v_{\mathrm{D}}$. For higher SNRs we observe that the adaptive subspace selection algorithm quickly reaches the performance of the fixed subspace selection if we increase $v_{\mathrm{D}}$. The reason is the too small number of observations in the time direction which results in a too small granularity of the number of selectable subspaces in time for the dimension selection in (24). The dotted lines in Fig. 3 show the simulation results if the user is scheduled for two consecutive subframes in time. Clearly, the adaptive subspace selection algorithm is able to gain over a wider range of the Doppler bandwidth compared to the fixed subspace selection algorithm if more subframes can be observed.

The results in Fig. 4 present the MSE performance on the pilot positions $\mathcal{P}$ of the adaptive subspace selection algorithm in the frequency domain. We set the DSD support to $\nu_{\mathrm{D}} = \nu_{\mathrm{Dmax}}$ and vary the PDP support range within $0 \leq \theta_{\mathrm{P}} \leq \theta_{\mathrm{Pmax}}$. This relates to a maximum excess delay of $\tau_{\mathrm{P}} \in (0, 4.7)\,\mu\mathrm{s}$. We assume that the user occupies the whole system bandwidth which means all pilot symbols are available for the subspace selection algorithm. The figure presents the MSE that is obtained with adaptive subspace selection, the MSE with maximum support and the MSE if $\theta_{\mathrm{Pmax}}$ is perfectly known. The selection algorithm is able to gain up to 7 dB compared to the maximum fixed subspace for small normalized delays $\theta_{\mathrm{P}}$.

Finally, Fig. 5 shows the FER versus the number of iterations for a fixed SNR $= 13\,\mathrm{dB}$. We utilize a 16-QAM symbol alphabet and a coding rate of $R$ = 0.479. We compare the FER obtained by adaptive subspace selection with the FER obtained for the fixed maximum subspace for relative velocities $v \in \{50, 200, 400\}$ km/h. For the simulations we assume that the user is scheduled for two consecutive subframes and uses the whole system bandwidth $B$. We simulate 1000 frames. The results show that with the adaptive subspace selection algorithm the number of iterations required to achieve a certain

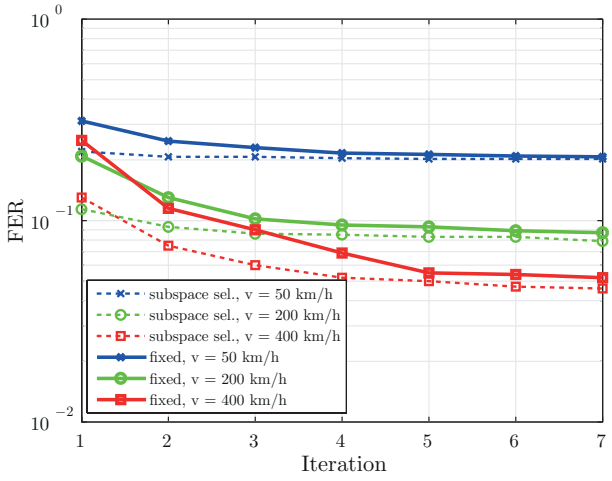


Fig. 5. FER vs. number of iterations for SNR $= 13$ dB and relative velocities $v \in \{50, 200, 400\}$ km/h; $R = 0.479$, 16-QAM symbol alphabet

FER can be reduced. For a velocity of $\{50, 200, 400\}$ km/h we need $\{-, 2, 2\}$ iterations to obtain a FER lower than $10^{-1}$. For fixed subspace $\{-, 4, 3\}$ iterations are required.

## VI. Conclusion

In this paper we presented an iterative channel estimator with an adaptive subspace selection algorithm for LTE communication that adapts to the current channel realization on a *per frame basis*. We modified the adaptive subspace selection algorithm that was presented for a contiguous pilot grid to a non-contiguous pilot grid and showed simulation results, especially concentrating on the LTE downlink pilot pattern. Furthermore, we adapted the iterative channel estimation algorithm to higher symbol alphabets. The results show that the performance of the adaptive subspace selection algorithm increases for larger observation regions, either in the time or in the frequency domain. This stresses the necessity of sophisticated scheduling and resource allocation algorithms for frame based communication. Furthermore, the adaptive subspace selection algorithm allows to reduce the number of required iterations to obtain a certain FER. This allows a complexity reduction of the implementation of the iterative channel estimator. Additionally, this frame based channel estimation technique could also be utilized for LTE D2D communication if the LTE downlink pilot pattern is assumed.

## Acknowledgments

This research was supported by the project NOWIRE funded by the Vienna Science and Technology Fund (WWTF), the project NFN SISE (S10607) funded by the Austrian Science Fund (FWF) as well as the strategic FTW project I-0. The Austrian Competence Center FTW Forschungszentrum Telekommunikation Wien GmbH is funded within the program COMET - Competence Centers for Excellent Technologies by BMVIT, BMWFJ, and the City of Vienna. The COMET program is managed by the FFG.

## References

[1] "ETSI TR 102 638 - Intelligent Transport Systems (ITS); Vehicular Communications; Basic Set of Applications; Definitions."

[2] "IEEE Standard for Information Technology–Telecommunications and Information Exchange between Systems Local and Metropolitan Area Networks–Specific Requirements Part 11: Wireless LAN Medium Access Control (MAC) and Physical Layer (PHY) Specifications," *IEEE Std 802.11-2012 (Revision of IEEE Std 802.11-2007)*, pp. 1–2793, 2012.

[3] 3GPP, "Technical Specification Group Radio Access Network; (E-UTRA) and (E-UTRAN); Overall Description; stage 2," Tech. Rep., Sep. 2008. [Online]. Available: http://www.3gpp.org/ftp/Specs/html-info/36300.htm

[4] G. Araniti, C. Campolo, M. Condoluci, A. Iera, and A. Molinaro, "LTE for Vehicular Networking: A Survey," *IEEE Communications Magazine*, vol. 51, no. 5, pp. 148–157, 2013.

[5] A. Molisch, F. Tufvesson, J. Karedal, and C. Mecklenbrauker, "A Survey on Vehicle-to-Vehicle Propagation Channels," *IEEE Wireless Communications*, vol. 16, no. 6, pp. 12–22, 2009.

[6] C. Mecklenbrauker, A. Molisch, J. Karedal, F. Tufvesson, A. Paier, L. Bernado, T. Zemen, O. Klemp, and N. Czink, "Vehicular Channel Characterization and Its Implications for Wireless System Design and Performance,," *Proceedings of the IEEE*.

[7] L. Bernadó, T. Zemen, F. Tufvesson, A. Molisch, and C. Mecklenbräuker, "Delay and Doppler Spreads of Non-Stationary Vehicular Channels for Safety Relevant Scenarios," 2013, to appear.

[8] T. Zemen and C. Mecklenbrauker, "Time-Variant Channel Estimation Using Discrete Prolate Spheroidal Sequences," *IEEE Transactions on Signal Processing*, vol. 53, no. 9, pp. 3597–3607, 2005.

[9] T. Zemen, L. Bernado, N. Czink, and A. Molisch, "Iterative Time-Variant Channel Estimation for 802.11p Using Generalized Discrete Prolate Spheroidal Sequences," *IEEE Transactions on Vehicular Technology*, vol. 61, no. 3, pp. 1222–1233, 2012.

[10] D. Slepian, "Prolate Spheroidal Wave Functions, Fourier Analysis, and Uncertainty - V: The Discrete Case," *The Bell System Technical Journal*, vol. 57, no. 5, pp. 1371–1430, May-June 1978.

[11] T. Zemen, C. Mecklenbrauker, F. Kaltenberger, and B. Fleury, "Minimum-Energy Band-Limited Predictor With Dynamic Subspace Selection for Time-Variant Flat-Fading Channels," *IEEE Transactions on Signal Processing*, vol. 55, no. 9, pp. 4534–4548, 2007.

[12] T. Zemen and A. Molisch, "Adaptive Reduced-Rank Estimation of Nonstationary Time-Variant Channels Using Subspace Selection," *IEEE Transactions on Vehicular Technology*, vol. 61, no. 9, pp. 4042–4056, 2012.

[13] S. Beheshti and M. A. Dahleh, "A new information-theoretic approach to signal denoising and best basis selection," vol. 53, no. 10, pp. 3613–3624, October 2005.

[14] 3GPP, "Technical Specification Group Radio Access Network; (E-UTRA) and (E-UTRAN); Physical Channels and Modulation; (Release 8)," Tech. Rep., Sep. 2008. [Online]. Available: http://www.3gpp.org/ftp/Specs/html-info/36211.htm

[15] C. Studer, M. Wenk, A. Burg, and H. Bolcskei, "Soft-Output Sphere Decoding: Performance and Implementation Aspects," in *Fortieth Asilomar Conference on Signals, Systems and Computers, 2006. ACSSC '06.*, 2006, pp. 2071–2076.

[16] T. Zemen, C. Mecklenbrauker, J. Wehinger, and R. Muller, "Iterative Joint Time-Variant Channel Estimation and Multi-User Detection for MC-CDMA," *IEEE Transactions on Wireless Communications*, vol. 5, no. 6, pp. 1469–1478, 2006.

[17] M. Tuechler, A. Singer, and R. Koetter, "Minimum Mean Squared Error Equalization Using A Priori Information," *Signal Processing, IEEE Transactions on*, vol. 50, no. 3, pp. 673–683, 2002.

[18] W. Haselmayr, D. Schellander, and A. Springer, "Iterative Channel Estimation and Turbo Equalization for Time-Varying Channels in a Coded OFDM-LTE System for 16-QAM and 64-QAM," in *IEEE 21st International Symposium on Personal Indoor and Mobile Radio Communications (PIMRC), 2010*, 2010, pp. 614–618.